

## Realization of flat bands by lattice intercalation in kagome metals

Dongwook Kim and Feng Liu\*

Department of Materials Science and Engineering, University of Utah, Salt Lake City, Utah 84112, USA

 (Received 2 December 2022; revised 17 April 2023; accepted 21 April 2023; published 16 May 2023)

Recently there has been intense interest in kagome metals, which are expected to host flat bands (FBs). However, the observed “FBs” are not flat over the whole two-dimensional Brillouin zone and overlap strongly with other bands. In fact, the FB does not truly exist in a default  $d$ -orbital kagome lattice, and the conditions for its existence in kagome metals are unknown. Here, based on tight-binding model analyses of the interplay between orbital and lattice symmetry, we establish such conditions. We show that for a single  $d$ -orbital kagome lattice assuming large crystal field splitting (CFS), only the  $d_{z^2}$  orbital gives rise to a FB, while  $d_{xy}$ ,  $d_{x^2-y^2}$ ,  $d_{xz}$ , and  $d_{yz}$  orbitals can only produce a FB with a rotated  $d$ -orbital basis so that they conform with the underlying kagome lattice symmetry. Most importantly, we demonstrate that both conditions of  $d$ -orbital rotation and large CFS can be ideally satisfied by intercalating the kagome lattice with a hexagonal sublattice without disrupting the destructive interference of FB wave function. Furthermore, we propose layered metalorganic frameworks as promising candidate kagome metals to realize FBs.

DOI: [10.1103/PhysRevB.107.205130](https://doi.org/10.1103/PhysRevB.107.205130)

### I. INTRODUCTION

The kagome lattice is arguably the most intriguing lattice. A spin kagome lattice is a prominent candidate for quantum spin liquid (QSL) due to geometrical frustration, while the quasiparticle eigenspectra of a kagome lattice contain an eigenvalue with macroscopic degeneracy, a flat band (FB), due to destructive quantum interference, i.e., phase cancellation of Bloch wave function. Hybrid kagome metals, namely, compounds containing layers of kagome sublattice of transition metals (TMs) sandwiched by layers of organic ligands have been long investigated to search for signatures of QSL [1–6], as well as other magnetic quantum states, such as quantum optical spin ice [7–11], kagome magnets [4,12,13], anomalous Hall effect [14], and skyrmions [15].

Recently, inorganic kagome metals, such as  $\text{CoSn}$ ,  $\text{Fe}_3\text{Sn}_2$ ,  $\text{CsV}_3\text{Sb}_5$ ,  $\text{YCr}_6\text{Ge}_6$ , and  $\text{Ni}_3\text{In}$ , have drawn increasing attention, due to the presence of Dirac bands with Van Hove singularities and the expected FB, which lead to a range of observed interesting physical phenomena, such as ferromagnetism [16–20] and superconductivity [21–24]. However, the experimentally observed FBs [25–29] as well as the density functional theory (DFT) calculated band structures are at best, if existent, nonideal, as they are not flat over the whole 2D Brillouin zone and buried with strong overlap with many other bands around the Fermi level [25–29]. Moreover, there remain fundamental gaps in our understanding of  $d$ -orbital FBs in kagome metals. Most critically, the FB does not truly exist in a default  $d$ -orbital kagome lattice [see Figs. S1(a) and S1(b) in the Supplemental Material (SM) [30], different from the simplest kagome lattice model assuming an  $s$  orbital per lattice site, and the conditions for its existence in kagome metals are unknown. Therefore, it is highly desirable to establish viable physical conditions for the emergence of

FB in kagome metals, which will open a promising avenue to realizing some elusive predicted FB phenomena, such as the fractional Quantum Hall effect (QHE) [31–36], Wigner crystallization [37–40], excitonic insulator [41,42], and the Quantum anomalous Hall (QAH)/Quantum spin Hall (QSH) effect [43–46].

In this paper, we develop a full tight-binding (TB)  $d$ -orbital kagome lattice model, to establish orbital rotation and large crystal field splitting (CFS) as general physical conditions for the existence of FBs in kagome metals, and most importantly demonstrate *hexagonal lattice intercalation* as an effective means to simultaneously satisfy both conditions. We show that in a single  $d$ -orbital kagome lattice model assuming a large CFS, only a  $d_{z^2}$  orbital by default gives rise to a FB; while  $d_{xy}$ ,  $d_{x^2-y^2}$ ,  $d_{xz}$ , and  $d_{yz}$  orbitals will only produce a FB is in a rotated basis so that they conform with the kagome lattice symmetry. Interestingly, the lattice having rotated  $d_{xy}$  ( $d_{xz}$ ) and  $d_{x^2-y^2}$  ( $d_{yz}$ ) orbitals leads to a FB of opposite chirality sitting above and below the Dirac bands, respectively. For intercalated TM kagome lattice planes, the kagome-hexagonal intercalation always exhibits an ideal FB, while the case for the kagome-trigonal intercalation is conditional depending on the interaction between the two sublattices. Our findings explain why all the currently known inorganic kagome metals do not have an isolated fully flat FB (see, e.g., Figs. S1(c) and S1(d) in the SM [30]). Furthermore, we propose layered metalorganic frameworks (MOFs) to be a family of kagome metals hosting FBs.

### II. TIGHT-BINDING MODEL OF A SINGLE ROTATED $d$ -ORBITAL KAGOME LATTICE

It is important to recognize that the basic kagome lattice model assumes by default a single  $s$  or  $p_z$  orbital of even parity sitting at each lattice site [16,47–51]. The FB arises from purely lattice symmetry, such as underlined by the line-graph theorem [52–55]. When five  $d$  orbitals are placed on

\*fliu@eng.utah.edu

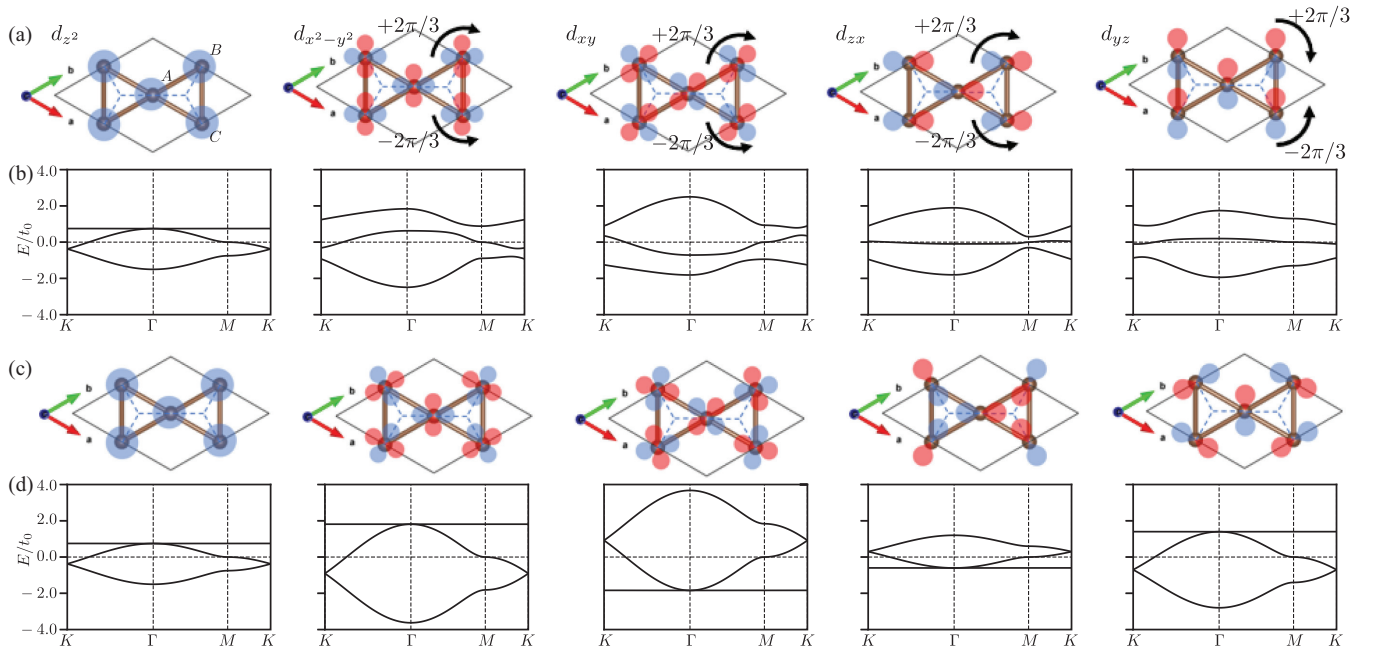


FIG. 1. Single  $d$ -orbital rotation in kagome lattice to form topological FB. (a) Schematic diagram of single  $d$  orbital with default orientation ( $d_z$ ,  $d_{x^2-y^2}$ ,  $d_{xy}$ ,  $d_{zx}$ , and  $d_{yz}$ ) and corresponding (b) TB band structures. (c) Conceptual diagram of rotated  $d$ -orbital basis [indicated by black arrows in (a)] and corresponding (d) TB band structures. Red and blue dots represent the positive and negative nodes of  $d$ -orbital wave functions.

each lattice site [Fig. S1(a) in the SM [30]], however, the FB diminishes [Fig. S1(b) in the SM [30]] due to the following complications. First, the five  $d$  orbitals have distinct symmetries; each of them alone may not conform with the underlying kagome lattice symmetry. Secondly, unlike the  $s$ - $s$  orbital hopping that is isotropic, inter- $d$ -orbital hopping is directional dependent, affecting the existence of the FB. Thirdly, the atomic TM  $d$  orbitals have a fivefold degeneracy; when the CFS is weak, the inter- $d$ -orbital hopping changes each individual subset of  $d$  bands and also causes overlap between them. Therefore, the existence of FBs in kagome metals is rather nontrivial, much beyond the commonly perceived simple kagome lattice model.

To concretely illustrate the above points, we develop a full TB  $d$ -orbital kagome lattice model, by explicitly implementing the five  $d$ -orbital symmetries to calculate band structure. For clarity and simplicity, we place one single  $d$  orbital on each kagome lattice site, which corresponds to the condition of a very large CFS. Figure 1(a) shows the schematic diagrams of a kagome lattice having the  $d_z$ ,  $d_{x^2-y^2}$ ,  $d_{xy}$ ,  $d_{zx}$ , and  $d_{yz}$  orbitals in their default orientations, respectively. Figure 1(b) shows the corresponding calculated band structures. One sees that only the  $d_z$ -orbital kagome lattice produces a perfect FB, while all other four orbitals fail. This is because the inter- $d_z$ -orbital hopping within the 2D plane is isotropic. In other words, the  $d_z$  orbital symmetry conforms with the underlying kagome lattice symmetry, the same as for the  $s$  or  $p_z$  orbital. In contrast, the other four orbitals have a twofold rotation symmetry which does not conform with the underlying lattice symmetries, e.g.,  $C_3 + T$ , and the interatomic hopping between them is anisotropic and directional dependent.

Consequently, these four  $d$ -orbital symmetries interfere with the kagome lattice symmetry to disrupt the condition of phase cancellation of the Bloch wave function [56] and hence to mitigate the FB.

We note that in the above calculations [Fig. 1(b)], we used typical hopping strength ( $V_{dd\sigma} = -1.20t_0$ ,  $V_{dd\pi} = +0.90t_0$ , and  $V_{dd\delta} = -0.10t_0$ ) for TM metals [57] in the Slater-Koster formalism [58]. Due to the nature of localized  $d$  orbitals, bandwidths are generally narrow and some appear rather “flat” [see the middle band in the last two columns of Fig. 1(b)], but they are isolated bands, different from the *topological* FB hosted in the kagome lattice, which has a singular band touching point with a dispersive Dirac band [16,47–55,59].

Therefore, a kagome lattice with default  $d$ -orbital orientations, and hence a kagome metal, does not generally host a topological FB, as commonly perceived. We found that an effective way to make the other four  $d$  orbitals conform with the kagome lattice symmetry is to rotate two of the three  $d$  orbitals clockwise/counterclockwise by a degree of  $2\pi/3$  within a unit cell, so that they conform with the threefold rotation among the three sublattice sites A, B, and C [marked in the first column of Fig. 1(a)] plus translation in the kagome lattice. Starting from the default  $d$ -orbital orientation in Fig. 1(a), we rotate two of them clockwise/counterclockwise by  $2\pi/3$ , as indicated by the curved black arrows, to arrive at the configuration of the rotated  $d$ -orbital basis in Fig. 1(c). Now they all produce an ideal FB, as shown in Fig. 1(d). Interestingly, one also sees that the lattice having rotated  $d_{x^2-y^2}/d_{xy}$  orbitals [the second/third column in Fig. 1(d)] leads to a FB of opposite chirality sitting above/below the Dirac bands, respectively [similarly for  $d_{zx}/d_{yz}$  orbitals in the fourth/fifth column of

Fig. 1(d)]. This means that due to the directional dependence of  $d$ -orbital hopping there are two groups of  $d$ -orbital kagome lattices that effectively have the lattice hopping of opposite sign ( $\pm t$ ) [59]. Also, we emphasize that the FB resulting from the rotated  $d$ -orbital kagome lattices as shown in Fig. 1(d) is symmetry protected and hence robust, independent of variations of hopping strength ( $V_{dd\sigma}$ ,  $V_{dd\pi}$ , and  $V_{dd\delta}$ ).

### III. LATTICE INTERCALATION INDUCED ORBITAL ROTATION

The reason for the above ‘‘hypothetically’’ rotated  $d$  orbital in a kagome lattice to produce a FB can be easily understood, from a theoretical point of view, because it effectively makes the inter- $d$ -orbital nearest-neighbor (NN) hopping become the same, as in the  $s$ -orbital kagome lattice (see Table S1 and related discussion in the SM [30]). However, how to rotate an isolated single  $d$  orbital, especially in a real material, is highly nontrivial. One has to find a way to not only rotate two out of three orbitals in the desired manner but also eliminate the hopping between different  $d$  orbitals by lifting their degeneracy. Remarkably, we found that this can be ideally done by hexagonal lattice intercalation.

Since the objective is to rotate the  $d$  orbital to conform with the  $C_3 + T$  symmetry of the kagome lattice, we intuitively tried hexagonal and trigonal lattice intercalation. For simplicity, assuming one  $s$  orbital at each site of the hexagonal [Fig. 2(a)] and triangular sublattice [Fig. 2(b)], the calculated bands are shown in Figs. 2(c) and 2(d), respectively, for varying on-site energy differences ( $\Delta_{sd} = \varepsilon_s - \varepsilon_d$ ) and interaction strength ( $V_{sd\sigma}$ ) between  $s$  and  $d$  orbitals. Here we show the case of  $d_{x^2-y^2}$  in Fig. 2 for illustration, and the other cases are shown in Fig. S2 in the SM [30] with qualitatively the same behavior. Red and blue bands present the intercalation-sublattice and kagome-sublattice projection, respectively. The TB bands obtained with two sets of representative limiting-case parameters [( $\Delta_{sd} = 10t_0$ ,  $V_{ss\sigma} = -1.2t_0$ ,  $V_{sd\sigma} = 0$ ) and ( $\Delta_{sd} = 0$ ,  $V_{ss\sigma} = -1.2t_0$ ,  $V_{sd\sigma} = 4t_0$ )] are shown in the upper and lower panels of Figs. 2(c) and 2(d), respectively (another intermediate case is shown in Fig. S2 in the SM [30]).

Most significantly, with the hexagonal intercalation [Fig. 2(c)], an ideal FB emerges all the time, consistent with the rotated  $d$ -orbital kagome bands modeled above, independent of  $V_{sd\sigma}$  and  $\Delta_{sd}$ . Even when  $\Delta_{sd}$  is small, the  $d$  bands of the kagome sublattice will inevitably overlap with the  $s$ -Dirac bands of the hexagonal sublattice; still the FB remains perfectly flat over the whole BZ [lower panel of Fig. 2(c)]. In contrast, the trigonal intercalation is less effective; the FB becomes dispersive and mixed with other bands when  $\Delta_{sd}$  is small [lower panel of Fig. 2(d)].

### IV. COMPATIBILITY OF LATTICE INTERCALATION WITH FB WAVE FUNCTION

The intriguing difference between the hexagonal versus triangular lattice intercalation in preserving the FB is revealed to be profoundly related to the fundamental nature of destructive quantum interference of the Bloch state in a kagome lattice, namely, the phase cancellation of outward hopping from the

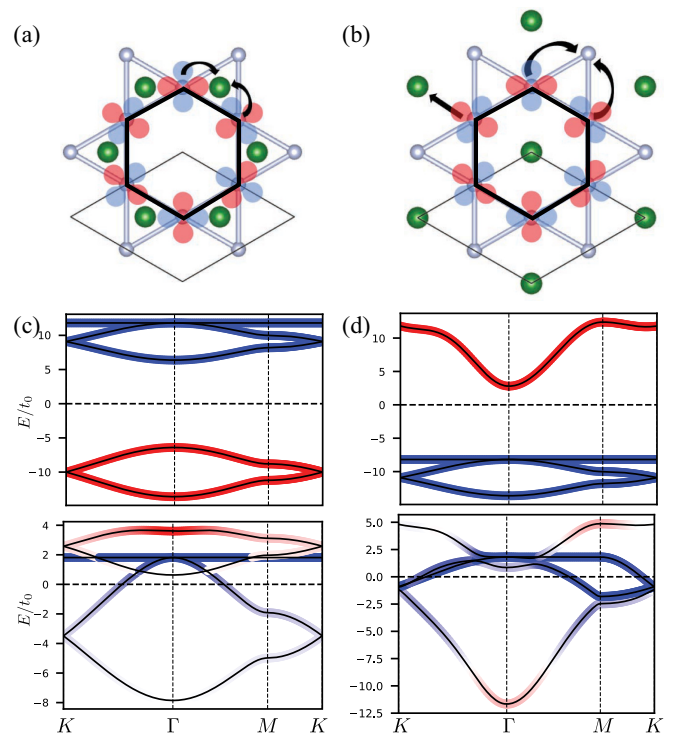


FIG. 2. Illustration of lattice intercalation (green balls) induced  $d_{x^2-y^2}$ -orbital (red and blue) rotation and compatibility of intercalation with FB wave function. (a) Kagome-hexagonal intercalated lattice and (b) kagome-trigonal intercalated lattice. Thin black rhombus indicates the unit cell. Black arrows indicate the outward NN hopping from CLS (thick black hexagon). (c), (d) TB band structures of kagome-hexagonal and -triangular intercalated lattice, respectively. Upper panels in (d), (e) show bands with on-site energy difference  $\Delta_{sd} = 10t_0$  and  $s-d$  hopping integrals  $V_{sd\sigma} = 0$ ; the lower shows bands with  $\Delta_{sd} = 0$  and  $V_{sd\sigma} = 4t_0$ . Blue and red bands represent the orbital projection onto the rotated  $d$ -orbital kagome and  $s$ -orbital intercalation sublattice, respectively.

real-space compact localized state (CLS) of FB wave function. To illustrate this point, in Figs. 2(a) and 2(b) we draw the outward hopping pattern from the CLS formed by the rotated  $d_{x^2-y^2}$ -orbital FB on the TM kagome lattice (silver balls) in the presence of a hexagonal and triangular intercalation lattice (green balls), respectively. Black arrows indicate the outward hopping from the CLS to the NN sites. The alternating positive and negative phases of  $d$  orbitals on six nodes of the CLS (marked by a black hexagon) are indicated in Figs. 2(a) and 2(b). It ensures the condition of phase cancellation for outward hopping from the CLS to all NN sites to vanish, so that the FB forms inherently in a kagome lattice without intercalation. In the presence of an additional intercalated lattice, one can see from the pattern of NN hopping, the condition for phase cancellation is still preserved by symmetry with the hexagonal lattice intercalation [paired curved black arrows in Fig. 2(a)]; namely, the hexagonal sublattice does not perturb the CLS outward hopping pattern, but not with the triangular intercalation [single straight black arrow in Fig. 2(b)]. In other words, the triangle lattice intercalation would disrupt the destructive interference of FB wave function, even though it could rotate the  $d$  orbital.

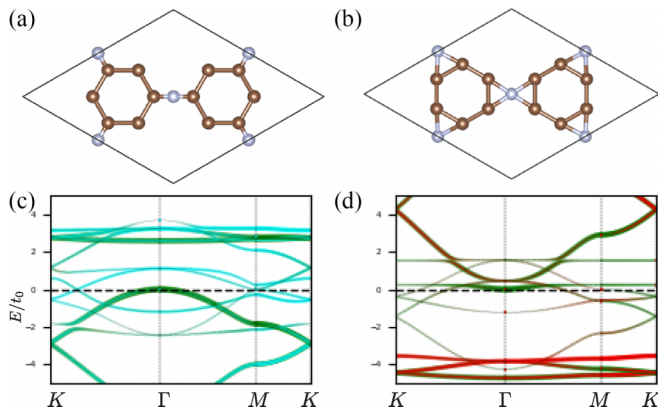


FIG. 3. Illustration of hexagonal intercalation motifs on effectively rotating the default  $d_{x^2-y^2}$  and  $d_{xy}$  orientations in the kagome lattice and enhancing CFS. (b), (c) Schematics of benzene-derived molecule intercalation. (c), (d) TB band structures with default  $d$  orbitals corresponding to atomic structure of (a), (b), respectively. Orbital projection of bands onto the rotated  $d_{x^2-y^2}$  and  $d_{xy}$  orbital basis is shown by cyan and red, respectively, indicating clearly the effect of orbital rotation induced by hexagonal intercalation. Green dotted bands are orbital projection onto the hexagonal intercalation lattice.

## V. EFFECT OF CRYSTAL FIELD SPLITTING

In the above analyses, we consider only one  $d$  orbital per kagome lattice site, which corresponds to the limit of a large CFS so that this  $d$  band is energetically well separated from other  $d$  bands. In real kagome metals, the CFS can vary. In addition to  $d$ -orbital rotation, another general condition for the emergence of a FB is to have a strong enough CFS ( $\Delta_0$ ) exceeding the bandwidth ( $W$ ), namely,  $\Delta_0 \gg W$  (see Fig. S3 and related discussion in the SM [30]). CFS is determined by local point-group symmetry of atoms (or molecular motifs) coordinated with the center TM atom and their bonding strength. The former dictates the lifted  $d$ -level degeneracy, while the latter affects the magnitude of energy splitting. When  $\Delta_0 \gg W$ , the isolation of  $d$  orbitals also makes the orbital rotation more effective by suppressing the inter- $d$ -orbital hopping.

One way to tune CFS is by changing the intercalation potential, such as by placing a benzene-derived molecule at each hexagonal sublattice site instead of a single atom, as shown in Fig. 3. Remarkably, the conditions of orbital rotation and  $\Delta_0 \gg W$  are found to be satisfied simultaneously by the intercalation with a strong ligand field, as revealed by TB calculation. Figures 3(a) and 3(b) show a case study of such intercalated kagome lattice. We place three degenerate  $d$  orbitals ( $\varepsilon_{d_{x^2-y^2}} = \varepsilon_{d_{xy}} = \varepsilon_{d_z} = 0$ ) in their default orientation, i.e., without rotation. These three  $d$  orbitals are orthogonal to other two  $d$  orbitals ( $\varepsilon_{d_{yz}}$  and  $\varepsilon_{d_{zx}}$ ) and the two groups have opposite mirror parity eigenvalues; therefore, the latter two are neglected without loss of generality. Two different orientations of benzene-derived molecules are considered as shown in Figs. 3(a) and 3(b), respectively, to account for different CFS due to different local bonding geometry. Figures 3(c) and 3(d) show the TB band structures corresponding to Figs. 3(a) and 3(b), respectively. In all cases, typical hopping strengths

( $V_{dd\sigma} = -1.20t_0$ ,  $V_{dd\pi} = +0.90t_0$ , and  $V_{dd\delta} = -0.10t_0$ ) are used again.  $V_{ss\sigma} = 16t_0$  is used for stronger interaction within the molecule, and  $V_{sd\sigma} = 4t_0$  is used between the kagome and hexagonal sublattices.

One sees that for both molecular orientations, the  $d$  bands from the kagome lattice are forming an identifiable FB, while a set of Dirac bands can be distinguished arising from the hexagonal sublattice. By purposely projecting bands onto the rotated  $d$  basis rather than the default basis, one reveals also the FB arises from the rotated  $d_{x^2-y^2}$  orbital (cyan) in Fig. 3(c) but the  $d_{xy}$  orbital (red) in Fig. 3(d), due to different molecular orientations that change their local bonding geometry and strength with the TM to modify the CFS. In contrast, as shown in Fig. 2(c), the single-atom intercalation is not able to modulate the flat band via changing  $V_{sd\sigma}$ . These results indicate that hexagonal intercalation with a strong ligand field can promote FB formation in a kagome metal by simultaneously rotating the  $d$  orbital and increasing CFS. Also, a larger intercalation molecule and a stronger intercalation potential are preferable for increasing CFS.

## VI. REALIZATION OF ROTATED $d$ -ORBITAL FB IN MOF KAGOME METAL

Finally, we present the electronic band structures of real materials using DFT calculations [60–63] to confirm the above theoretical findings. TM kagome lattices are often

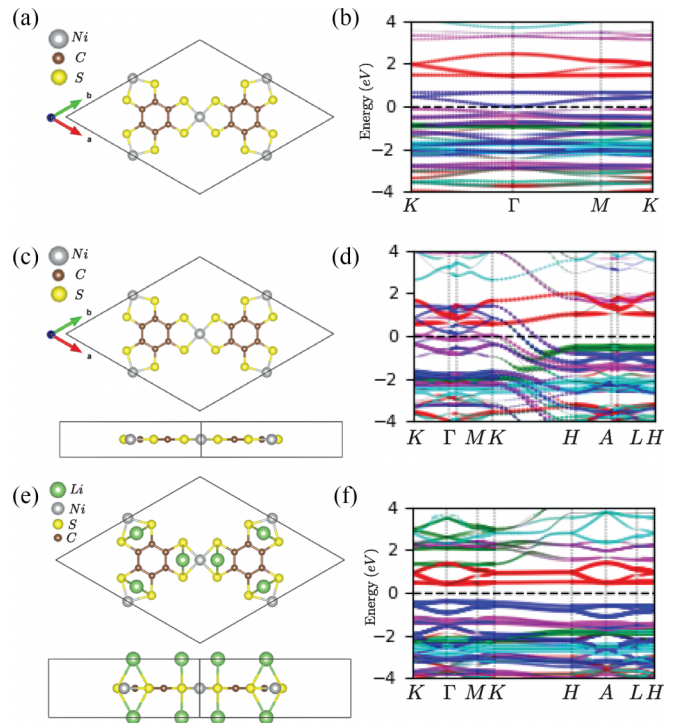


FIG. 4. Comparison between single stacking and alkali atom-intercalated layered 3D MOF metals. (a) Crystal structure and (b) DFT band structure of 2D  $\text{Ni}_3\text{C}_{12}\text{S}_{12}$ . (c) Crystal structure and (d) DFT band structure of AA stacked  $\text{Ni}_3\text{C}_{12}\text{S}_{12}$ . (e) Crystal structure and (f) DFT band structure of Li intercalation ( $\text{Ni}_3\text{C}_{12}\text{S}_{12}-\text{Li}_6$ ). Orbital projections onto the rotated  $d_z$ ,  $d_{x^2-y^2}$ ,  $d_{xy}$ ,  $d_{yz}$ , and  $d_{zx}$  orbitals are colored green, cyan, red, magenta, and blue, respectively.

TABLE I. Analysis of crystal structure of inorganic kagome metals. Intra- and interlayer intercalations with kagome TM sublattice are specified.

	Intralayer intercalation	Intercalation motif	Interlayer intercalation	FB existence
CoSn	Triangular	Sn	[Hexagonal Sn] $\times 2$	No
$AV_3Sb_5$ ( $A = K, Cs, Rb$ )	Triangular	Sb	[Triangular A] $\times 2$	No
GdV <sub>6</sub> Sn <sub>6</sub>	None	None	[Hexagonal Sb] $\times 2$ [Triangular Gd/Y + hexagonal Sn/Ge] [Triangular Sn/Ge] $\times 2$ [hexagonal Sn/Ge]	No
YCr <sub>6</sub> Ge <sub>6</sub>				
Ni <sub>3</sub> In	Triangular	In	[Triangular In + kagome TM] $\times 2$	No
Fe <sub>3</sub> Sn <sub>2</sub>	Triangular	Sn	[Hexagonal Sn] $\times 2$	No
Ni <sub>3</sub> C <sub>12</sub> S <sub>12</sub> - Li <sub>6</sub>	Hexagonal	C <sub>6</sub> S <sub>6</sub>	[Kagome TM + triangular Sn] $\times 2$ [Hexagonal Li <sub>3</sub> ] $\times 2$	Yes

found in two material systems, inorganic and MOF kagome metals. Our studies point to the need for an in-plane hexagonal intercalation of molecular motifs. By examining the known inorganic kagome metals (see Figs. S4 and S5 in the SM [30], and Table I), we found GdV<sub>6</sub>Sn<sub>6</sub>/YCr<sub>6</sub>Ge<sub>6</sub> do not have an in-plane intercalation lattice, while the others have a single-atom triangular intercalation lattice. Thus, the  $d$  orbital cannot be effectively rotated and the CFS is too small based on our theoretical analyses (Table I). This explains why they do not truly exhibit a topological FB, as commonly perceived. Instead, some 2D MOF structures are known to have a TM kagome lattice intercalated with a hexagonal lattice of benzene-derived motifs. Therefore, we propose layered MOF kagome metals to be a promising family of organic kagome metals to realize FB. This has been indeed confirmed by DFT calculations of an example system, Ni<sub>3</sub>C<sub>12</sub>S<sub>12</sub>-Li<sub>6</sub>, as shown in Fig. 4. A monolayer 2D MOF with a kagome TM sublattice, such as Ni<sub>3</sub>C<sub>12</sub>S<sub>12</sub>, is well known to host an ideal FB [48,64], as shown in Fig. 4(b), which can be understood by our analyses in Figs. 2 and 3. Now, in forming layered three-dimensional (3D) MOF kagome metals, if one simply stacks 2D MOF layers together, such as AA stacking shown in Fig. 4(c), then the FB in each individual 2D layer is heavily perturbed becoming dispersive [Fig. 4(d)] due to too strong interlayer interaction. To reduce the interlayer interaction, alkali metal intercalation can be used, such as Li intercalation [Fig. 4(e)], which will resume the FB [see red and blue dotted bands in Fig. 4(f)]. It is important to point out that such intercalation has been indeed observed in experiments [64,65]. Also, by

first-principles calculation, AA stacking is suggested as being energetically more stable than AB stacking [66,67]. We also perform orbital decomposition of DFT band structures by projecting onto the rotated  $d$  orbitals using the rotation matrix (Eq. (S5) in the SM [30]), to illustrate the effective  $d$ -orbital rotation by intercalation (see also Fig. S6 and related discussions in the SM [30]). This allows us to clearly show the FBs in MOF are composed of single rotated  $d$ -orbitals.

## VII. CONCLUSION

We have developed a TB model to establish the necessary conditions of  $d$ -orbital rotation and strong CFS for the emergence of topological FBs in kagome metals. Significantly, we demonstrate that these two conditions can and only can be simultaneously met by intercalating the kagome TM lattice plane with a hexagonal sublattice of molecular motifs, which are not fulfilled by any known existing inorganic kagome metal. Instead, we propose a family of layered MOF kagome metals as promising candidate materials for realizing the elusive topological FB.

## ACKNOWLEDGMENTS

This work is supported by U.S. DOE-BES (Grant No. DE-FG02-04ER46148). Support from the CHPC at the University of Utah and the NERSC at the Office of Science in the U.S. Department of Energy is gratefully acknowledged.

- [1] Y. Iqbal, F. Becca, S. Sorella, and D. Poilblanc, Gapless spin-liquid phase in the kagome spin- $\frac{1}{2}$  Heisenberg antiferromagnet, *Phys. Rev. B* **87**, 060405(R) (2013).
- [2] Z. A. Kelly, M. J. Gallagher, and T. M. McQueen, Electron Doping a Kagome Spin Liquid, *Phys. Rev. X* **6**, 041007 (2016).
- [3] M. Hermele, Y. Ran, P. A. Lee, and X.-G. Wen, Properties of an algebraic spin liquid on the kagome lattice, *Phys. Rev. B* **77**, 224413 (2008).
- [4] T.-H. Han, J. S. Helton, S. Chu, D. G. Nocera, J. A. Rodriguez-Rivera, C. Broholm, and Y. S. Lee, Fractionalized excitations

- in the spin-liquid state of a kagome-lattice antiferromagnet, *Nature (London)* **492**, 406 (2012).
- [5] Z. Liu, X. Zou, J.-W. Mei, and F. Liu, Selectively doping barlowite for quantum spin liquid: A first-principles study, *Phys. Rev. B* **92**, 220102(R) (2015).
- [6] Z. Feng, Z. Li, X. Meng, W. Yi, Y. Wei, J. Zhang, Y.-C. Wang, W. Jiang, Z. Liu, S. Li *et al.*, Gapped spin-1/2 spinon excitations in a new kagome quantum spin liquid compound Cu<sub>3</sub>Zn(OH)<sub>6</sub>FBr, *Chin. Phys. Lett.* **34**, 077502 (2017).

- [7] E. Mengotti, L. J. Heyderman, A. Fraile Rodríguez, A. Bisig, L. Le Guyader, F. Nolting, and H. B. Braun, Building blocks of an artificial kagome spin ice: Photoemission electron microscopy of arrays of ferromagnetic islands, *Phys. Rev. B* **78**, 144402 (2008).
- [8] Y. Qi, T. Brintlinger, and J. Cumings, Direct observation of the ice rule in an artificial kagome spin ice, *Phys. Rev. B* **77**, 094418 (2008).
- [9] E. Mengotti, L. J. Heyderman, A. F. Rodríguez, F. Nolting, R. V. Hügli, and H.-B. Braun, Real-space observation of emergent magnetic monopoles and associated Dirac strings in artificial kagome spin ice, *Nat. Phys.* **7**, 68 (2011).
- [10] W. Bang, J. Sturm, R. Silvani, M. T. Kaffash, A. Hoffmann, J. B. Ketterson, F. Montoncello, and M. B. Jungfleisch, Influence of the Vertex Region on Spin Dynamics in Artificial Kagome Spin Ice, *Phys. Rev. Appl.* **14**, 014079 (2020).
- [11] U. B. Arnalds, A. Farhan, R. V. Chopdekar, V. Kapaklis, A. Balan, E. Th. Papaioannou, M. Ahlberg, F. Nolting, L. J. Heyderman, and B. Hjörvarsson, Thermalized ground state of artificial kagome spin ice building blocks, *Appl. Phys. Lett.* **101**, 112404 (2012).
- [12] J.-X. Yin, S. S. Zhang, G. Chang, Q. Wang, S. S. Tsirkin, Z. Guguchia, B. Lian, H. Zhou, K. Jiang, I. Belopolski *et al.*, Negative flat band magnetism in a spin-orbit-coupled correlated kagome magnet, *Nat. Phys.* **15**, 443 (2019).
- [13] P. Khuntia, M. Velazquez, Q. Barthélemy, F. Bert, E. Kermarrec, A. Legros, B. Bernu, L. Messio, A. Zorko, and P. Mendels, Gapless ground state in the archetypal quantum kagome antiferromagnet  $\text{ZnCu}_3(\text{OH})_6\text{Cl}_2$ , *Nat. Phys.* **16**, 469 (2020).
- [14] T. Kida, L. A. Fenner, A. A. Dee, I. Terasaki, M. Hagiwara, and A. S. Wills, The giant anomalous Hall effect in the ferromagnet  $\text{Fe}_3\text{Sn}_2$ —a frustrated kagome metal, *J. Phys.: Condens. Matter* **23**, 112205 (2011).
- [15] Z. Hou, W. Ren, B. Ding, G. Xu, Y. Wang, B. Yang, Q. Zhang, Y. Zhang, E. Liu, F. Xu *et al.*, Observation of various and spontaneous magnetic skyrmionic bubbles at room temperature in a frustrated kagome magnet with uniaxial magnetic anisotropy, *Adv. Mater.* **29**, 1701144 (2017).
- [16] A. Mielke, Ferromagnetic ground states for the Hubbard model on line graphs, *J. Phys. A: Math. Gen.* **24**, L73 (1991).
- [17] A. Mielke, Ferromagnetism in the Hubbard model on line graphs and further considerations, *J. Phys. A: Math. Gen.* **24**, 3311 (1991).
- [18] A. Mielke, Exact ground states for the Hubbard model on the kagome lattice, *J. Phys. A: Math. Gen.* **25**, 4335 (1992).
- [19] H. Tasaki, Ferromagnetism in the Hubbard Models with Degenerate Single-Electron Ground States, *Phys. Rev. Lett.* **69**, 1608 (1992).
- [20] S. Zhang, H.-h. Hung, and C. Wu, Proposed realization of itinerant ferromagnetism in optical lattices, *Phys. Rev. A* **82**, 053618 (2010).
- [21] S. Miyahara, S. Kusuta, and N. Furukawa, BCS theory on a flat band lattice, *Phys. C (Amsterdam)* **460–462**, 1145 (2007).
- [22] K. Kobayashi, M. Okumura, S. Yamada, M. Machida, and H. Aoki, Superconductivity in repulsively interacting fermions on a diamond chain: Flat-band-induced pairing, *Phys. Rev. B* **94**, 214501 (2016).
- [23] G. E. Volovik, Graphite, graphene, and the flat band superconductivity, *JETP Lett.* **107**, 516 (2018).
- [24] J. S. Hofmann, E. Berg, and D. Chowdhury, Superconductivity, pseudogap, and phase separation in topological flat bands, *Phys. Rev. B* **102**, 201112(R) (2020).
- [25] M. Kang, L. Ye, S. Fang, J.-S. You, A. Levitan, M. Han, J. I. Facio, C. Jozwiak, A. Bostwick, E. Rotenberg *et al.*, Dirac Fermions and flat bands in the ideal kagome metal  $\text{FeSn}$ , *Nat. Mater.* **19**, 163 (2020).
- [26] Z. Lin, J.-H. Choi, Q. Zhang, W. Qin, S. Yi, P. Wang, L. Li, Y. Wang, H. Zhang, Z. Sun *et al.*, Flatbands and Emergent Ferromagnetic Ordering in  $\text{Fe}_3\text{Sn}_2$  Kagome Lattices, *Phys. Rev. Lett.* **121**, 096401 (2018).
- [27] L. Ye, M. Kang, J. Liu, F. von Cube, C. R. Wicker, T. Suzuki, C. Jozwiak, A. Bostwick, E. Rotenberg, D. C. Bell *et al.*, Massive Dirac fermions in a ferromagnetic kagome metal, *Nature (London)* **555**, 638 (2018).
- [28] B. R. Ortiz, S. M. L. Teicher, Y. Hu, J. L. Zuo, P. M. Sarte, E. C. Schueller, A. M. Milinda Abeykoon, M. J. Krogstad, S. Rosenkranz, R. Osborn *et al.*,  $\text{CsV}_3\text{Sb}_5$ : A  $Z_2$  Topological Kagome Metal with a Superconducting Ground State, *Phys. Rev. Lett.* **125**, 247002 (2020).
- [29] M. Kang, S. Fang, L. Ye, H. C. Po, J. Denlinger, C. Jozwiak, A. Bostwick, E. Rotenberg, E. Kaxiras, J. G. Checkelsky *et al.*, Topological flat bands in frustrated kagome lattice  $\text{CoSn}$ , *Nat. Commun.* **11**, 4004 (2020).
- [30] See Supplemental Material at <http://link.aps.org/supplemental/10.1103/PhysRevB.107.205130> for realization of the flat band by intercalation lattice in kagome metals, which contains Refs. [60–63].
- [31] E. Tang, J.-W. Mei, and X.-G. Wen, High-Temperature Fractional Quantum Hall States, *Phys. Rev. Lett.* **106**, 236802 (2011).
- [32] T. Neupert, L. Santos, C. Chamon, and C. Mudry, Fractional Quantum Hall States at Zero Magnetic Field, *Phys. Rev. Lett.* **106**, 236804 (2011).
- [33] Z. Liu, F. Liu, and Y.-S. Wu, Exotic electronic states in the world of flat bands: From theory to material, *Chin. Phys. B* **23**, 077308 (2014).
- [34] K. Sun, Z. Gu, H. Katsura, and S. Das Sarma, Nearly Flatbands with Nontrivial Topology, *Phys. Rev. Lett.* **106**, 236803 (2011).
- [35] D. N. Sheng, Z.-C. Gu, K. Sun, and L. Sheng, Fractional quantum Hall effect in the absence of Landau levels, *Nat. Commun.* **2**, 389 (2011).
- [36] Y.-F. Wang, H. Yao, C.-D. Gong, and D. N. Sheng, Fractional quantum Hall effect in topological flat bands with Chern number two, *Phys. Rev. B* **86**, 201101(R) (2012).
- [37] C. Wu and S. Das Sarma,  $p_{x,y}$ -orbital counterpart of graphene: Cold atoms in the honeycomb optical lattice, *Phys. Rev. B* **77**, 235107 (2008).
- [38] C. Wu, D. Bergman, L. Balents, and S. Das Sarma, Flat Bands and Wigner Crystallization in the Honeycomb Optical Lattice, *Phys. Rev. Lett.* **99**, 070401 (2007).
- [39] B. Jaworowski, A. D. Güçlü, P. Kaczmarkiewicz, M. Kupczyński, P. Potasz, and A. Wójs, Wigner crystallization in topological flat bands, *New J. Phys.* **20**, 063023 (2018).
- [40] Y. Chen, S. Xu, Y. Xie, C. Zhong, C. Wu, and S. B. Zhang, Ferromagnetism and Wigner crystallization in kagome graphene and related structures, *Phys. Rev. B* **98**, 035135 (2018).
- [41] D. Jérôme, T. M. Rice, and W. Kohn, Excitonic insulator, *Phys. Rev.* **158**, 462 (1967).

- [42] G. Sethi, Y. Zhou, L. Zhu, L. Yang, and F. Liu, Flat-Band-Enabled Triplet Excitonic Insulator in a Diatomic Kagome Lattice, *Phys. Rev. Lett.* **126**, 196403 (2021).
- [43] R. Chen and B. Zhou, Spin Chern number and topological phase transition on the Lieb lattice with spin-orbit coupling, *Phys. Lett. A* **381**, 944 (2017).
- [44] W.-F. Tsai, C. Fang, H. Yao, and J. Hu, Interaction-driven topological and nematic phases on the Lieb lattice, *New J. Phys.* **17**, 055016 (2015).
- [45] Z. F. Wang, Z. Liu, and F. Liu, Quantum Anomalous Hall Effect in 2D Organic Topological Insulators, *Phys. Rev. Lett.* **110**, 196801 (2013).
- [46] Y. Zhou, G. Sethi, H. Liu, Z. Wang, and F. Liu, Excited quantum anomalous and spin Hall effect: Dissociation of flat-bands-enabled excitonic insulator state, *Nanotechnology* **33**, 415001 (2022).
- [47] J.-W. Rhim and B.-J. Yang, Classification of flat bands according to the band-crossing singularity of Bloch wave functions, *Phys. Rev. B* **99**, 045107 (2019).
- [48] D.-S. Ma, Y. Xu, C. S. Chiu, N. Regnault, A. A. Houck, Z. Song, and B. A. Bernevig, Spin-Orbit-Induced Topological Flat Bands in Line and Split Graphs of Bipartite Lattices, *Phys. Rev. Lett.* **125**, 266403 (2020).
- [49] Y. Zong, S. Xia, L. Tang, D. Song, Y. Hu, Y. Pei, J. Su, Y. Li, and Z. Chen, Observation of localized flat-band states in kagome photonic lattices, *Opt. Express* **24**, 8877 (2016).
- [50] D. L. Bergman, C. Wu, and L. Balents, Band touching from real-space topology in frustrated hopping models, *Phys. Rev. B* **78**, 125104 (2008).
- [51] Z. Li, J. Zhuang, L. Wang, H. Feng, Q. Gao, X. Xu, W. Hao, X. Wang, C. Zhang, K. Wu *et al.*, Realization of flat band with possible nontrivial topology in electronic kagome lattice, *Sci. Adv.* **4**, eaau4511 (2018).
- [52] W. Jiang, X. Ni, and F. Liu, Exotic topological bands and quantum states in metal-organic and covalent-organic frameworks, *Acc. Chem. Res.* **54**, 416 (2021).
- [53] W. Jiang, M. Kang, H. Huang, H. Xu, T. Low, and F. Liu, Topological band evolution between Lieb and kagome lattices, *Phys. Rev. B* **99**, 125131 (2019).
- [54] C.-C. Lee, A. Fleurence, Y. Yamada-Takamura, and T. Ozaki, Hidden mechanism for embedding the flat bands of Lieb, kagome, and checkerboard lattices in other structures, *Phys. Rev. B* **100**, 045150 (2019).
- [55] B. Pal, Nontrivial topological flat bands in a diamond-octagon lattice geometry, *Phys. Rev. B* **98**, 245116 (2018).
- [56] H. Liu, G. Sethi, S. Meng, and F. Liu, Orbital design of flat bands in non-line-graph lattices via line-graph wave functions, *Phys. Rev. B* **105**, 085128 (2022).
- [57] K. Masuda, N. Hamada, and K. Terakura, Calculation of elastic constants of bcc transition metals: Tight-binding recursion method, *J. Phys. F: Met. Phys.* **14**, 47 (1984).
- [58] J. C. Slater and G. F. Koster, Simplified LCAO method for the periodic potential problem, *Phys. Rev.* **94**, 1498 (1954).
- [59] Y. Zhou, G. Sethi, C. Zhang, X. Ni, and F. Liu, Giant intrinsic circular dichroism of enantiomorphic flat Chern bands and flatband devices, *Phys. Rev. B* **102**, 125115 (2020).
- [60] G. Kresse and J. Furthmüller, Efficiency of *ab-initio* total energy calculations for metals and semiconductors using a plane-wave basis set, *Comput. Mater. Sci.* **6**, 15 (1996).
- [61] H. J. J. Monkhorst and J. D. D. Pack, Special points for Brillouin-zone integrations, *Phys. Rev. B* **13**, 5188 (1976).
- [62] J. P. Perdew, K. Burke, and M. Ernzerhof, Generalized Gradient Approximation Made Simple [Phys. Rev. Lett. **77**, 3865 (1996)], *Phys. Rev. Lett.* **78**, 1396(E) (1997).
- [63] J. P. Perdew, K. Burke, and M. Ernzerhof, Generalized Gradient Approximation Made Simple, *Phys. Rev. Lett.* **77**, 3865 (1996).
- [64] Z. F. Wang, N. Su, and F. Liu, Prediction of a two-dimensional organic topological insulator, *Nano Lett.* **13**, 2842 (2013).
- [65] T. Kambe, R. Sakamoto, T. Kusamoto, T. Pal, N. Fukui, K. Hoshiko, T. Shimojima, Z. Wang, T. Hirahara, K. Ishizaka *et al.*, Redox control and high conductivity of nickel bis(dithiolene) complex  $\pi$ -nanosheet: A potential organic two-dimensional topological insulator, *J. Am. Chem. Soc.* **136**, 14357 (2014).
- [66] F. C. de Lima, G. J. Ferreira, and R. H. Miwa, Tuning the topological states in metal-organic bilayers, *Phys. Rev. B* **96**, 115426 (2017).
- [67] F. Crasto de Lima, G. J. Ferreira, and R. H. Miwa, Layertronic control of topological states in multilayer metal-organic frameworks, *J. Chem. Phys.* **150**, 234701 (2019).